Wind and Structures, *Vol. 19, No. 1 (2014) 000-000*
DOI: http://dx.doi.org/10.12989/was.2014.19.1.000

Numerical study on dynamics of a tornado-like vortex with touching down by using the LES turbulence model

Takeshi Ishihara* and Zhenqing Liu[a]

Department of Civil Engineering , School of Engineering, The University of Tokyo, 7-3-1 Hongou, Bunkyo-ku, Tokyo 113-8656, Japan

(Received September 10, 2012, Revised March 10, 2014, Accepted May 18, 2014)

Abstract. The dynamics of a tornado-like vortex with touching down is investigated by using the LES turbulence model. The detailed information of the turbulent flow fields is provided and the force balances in radial and vertical directions are evaluated by using the time-averaged axisymmetric Navier-Stokes equations. The turbulence has slightly influence on the mean flow fields in the radial direction whereas it shows strong impacts in the vertical direction. In addition, the instantaneous flow fields are investigated to clarify and understand the dynamics of the vortex. An organized swirl motion is observed, which is the main source of the turbulence for the radial and tangential components, but not for the vertical component. Power spectrum analysis is conducted to quantify the organized swirl motion of the tornado-like vortex. The gust speeds are also examined and it is found to be very large near the center of vortex.

Keywords: dynamics of tornado-like vortex with touching down; LES; turbulent flow fields; force balances; organized swirl motion; power spectrum; gust speed

1. Introduction

Tornadoes are vortices with strong three-dimensional flow fields and cause severe damages. Wind resistant design of structures requires proper consideration of tornado-induced wind loads and tornado-borne missiles, which requires detailed information of the three-dimensional flow fields of tornadoes.

In laboratory simulations, Ward (1972) first developed a tornado simulator with a fan at the top to generate updraft flow and guide-vanes near the floor to provide angular momentum, and succeeded in generation of many types of tornado-like vortices observed in nature. Wan and Chang (1972) measured the radial, tangential and vertical velocities with a three-dimensional velocity probe and provided a feasible supplement to field measurements of the natural tornado. Baker (1981) made the velocity measurements in a laminar vortex boundary layer by employing hot-film anemometry. Mitsuta and Monji (1984) modified the simulator so that the rotation is given at the top of the simulator, and showed the occurrence of the maximum tangential velocity near the ground in the two-cell type vortex. Haan *et al*. (2008) developed a large laboratory simulator with

*Corresponding author, Professor, E-mail: ishihara@bridge.t.u-tokyo.ac.jp
[a] Ph.D. Student, E-mail: liu@bridge.t.u-tokyo.ac.jp

http://www.techno-press.org/?journal=was&subpage=8 ISSN: 1226-6116 (Print), 1598-6225 (Online)

guide-vanes at the top to generate vortex. In their study, the measurements of the flow structure in the vortex were validated by comparing with mobile Doppler radar observations of two major tornadoes. Matsui and Tamura (2009) conducted the velocity measurements for tornado-like vortex generated by a Ward-type simulator with Laser Doppler Velocimeter (LDV). Recently, Tari *et al*. (2010) quantified both the mean and turbulent flow fields for a range of swirl ratios by using the Particle Image Velocimetry (PIV) method. They showed a critical swirl ratio, where the turbulent vortex touches down and the turbulent production approaches maximum values. In addition, they argued that close to the ground, the turbulence is responsible for the damage associated to tornado events. However, in laboratory simulations, it is difficult to make detailed three-dimensional measurements due to the strong turbulence near the surface and the corner of the vortex.

Numerical modeling paves the way for better understanding of tornadoes. Wilson and Rotunno (1986), Howells *et al*. (1988) and Nolan and Farrell (1999) used axisymmetric Navier-Stokes equation in cylindrical coordinates to investigate the flow fields of the tornado-like vortex as well as the dynamics in the boundary layer and corner regions. Kuai *et al*. (2008) used the k-ε model to study parameter sensitivity for the flow fields of a laboratory-simulated tornado. They proposed that the numerical approach can be used to simulate the surface winds of a tornado and to control certain parameters of the laboratory simulator. However, when the vortex experiences a "breakdown", the flow will be no longer axisymmetric, which means that dynamics of the vertex cannot be simulated with a two-dimensional axisymmetric model. Lewellen *et al*. (1997, 2000, 2007) used three-dimensional LES turbulence model to examine several types of tornado-like vortex, the influence of the translation speed as well as the interaction with the surface roughness. They proposed to use the local swirl ratio to identify the tornado structures, and it is found when $S_c \approx 2.0$, a sharp vortex breakdown caps a strong central jet forming a touching-down structure. The presence of vortex touching-down results in the largest swirl velocity occurring near the ground. Ishihara *et al*. (2011) investigated the detailed corner flow patterns of tornado-like vortices by using the LES turbulence model for two typical swirl ratios according to weak vortex and vortex touchdown, and the mechanism of the flow field formation was revealed by evaluating the axisymmetric time averaged Navier-Stokes equations. Most recently a large eddy simulation about the roughness effects on tornado-like vortices was carried out by Natarajan and Hangan (2012). The effects of the swirl ratio on the turbulent flow fields of tornado-like vortices were investigated by Liu and Ishihara (2012), in which, similar as the study by Lewellen *et al*. (2000), the vortex touching down status also occurs at $S_c \approx 2.0$. The studies by Lewellen *et al*. (2000, 2007) give similar overshooting profiles near the ground as for tangential and radial velocities as well as the large wind fluctuations near the center at the stage of vortex touching down, the mechanism of the large fluctuations, the spectra of fluctuating velocities and gust speeds in tornado-like vortices with touching-down have not been made clear.

In this study, a comprehensive study of the tornado-like vortex with touching down is performed by using LES turbulence model to shed light on the dynamics of a tornado-like vortex in the corner region where is of interest for engineering applications. Numerical model and configurations of a numerical Ward-type tornado simulator are described in section 2, including its dimension, grid distribution and boundary conditions. Section 3 aims to clarify the mean and turbulent characteristics of the vortex and to examine the force balances and the turbulent contribution to the mean flow by the axisymmetric time-averaged Navier-Stokes equations. Finally, the instantaneous flow field and the spectrum analysis are employed to examine the organized

motion in the tornado-like vortex with touching-down and the gust speeds are investigated to provide valuable information for the design purposes in section 4.

2. Numerical model

In this study, large eddy simulation (LES) is adopted to simulate the tornado-like vortex, in which large eddies are computed directly, while the influence of eddies smaller than grid spacing are modeled. Boussinesq hypothesis is employed and standard Smagorinsky-Lilly model is used to calculate the subgrid-scale (SGS) stresses.

2.1 Governing equations and boundary conditions

The governing equations are obtained by filtering the time-dependent Navier-Stokes equations in Cartesian coordinates (x, y, z) and expressed in the form of tensor as follows

$$\frac{\partial \rho \tilde{u}_i}{\partial x_j} = 0 \tag{1}$$

$$\frac{\partial \rho \tilde{u}_i}{\partial t} + \frac{\partial \rho \tilde{u}_i \tilde{u}_j}{\partial x_j} = \frac{\partial}{\partial x_j}\left(\mu \frac{\partial \tilde{u}_i}{\partial x_j}\right) - \frac{\partial \tilde{p}}{\partial x_i} - \frac{\partial \tau_{ij}}{\partial x_j} \tag{2}$$

where, $\tilde{u}_i$ and $\tilde{p}$ are filtered velocities and pressure respectively, μ is the viscosity, ρ is air density, τ_{ij} is SGS stress and is modeled as follows

$$\tau_{ij} = -2\mu_t \tilde{S}_{ij} + \frac{1}{3}\tau_{kk}\delta_{ij}, \qquad \tilde{S}_{ij} = \frac{1}{2}\left(\frac{\partial \tilde{u}_i}{\partial x_j} + \frac{\partial \tilde{u}_j}{\partial x_i}\right) \tag{3}$$

where μ_t denotes SGS turbulent viscosity, and $\tilde{S}_{ij}$ is the rate-of-strain tensor for the resolved scale, δ_{ij} is the Kronecker delta. Smagorinsky-Lilly model is used for the SGS turbulent viscosity

$$\mu_t = \rho L_S^2 \left|\tilde{S}\right| = \rho L_S \sqrt{2\tilde{S}_{ij}\tilde{S}_{ij}}; \qquad L_S = \min\left(\kappa d, C_S V^{\frac{1}{3}}\right) \tag{4}$$

in which, L_S denotes the mixing length for subgrid-scales, κ is the von Kármán constant, 0.42, d is the distance to the closest wall and V is the volume of a computational cell. In this study, Smagorinsky constant, C_S, is determined as 0.032 based on Oka and Ishihara (2009)

For the wall-adjacent cells, the wall shear stresses are obtained from the laminar stress-strain relationship in the laminar sublayer

$$\frac{\tilde{u}}{u_\tau} = \frac{\rho u_\tau y}{\mu} \tag{5}$$

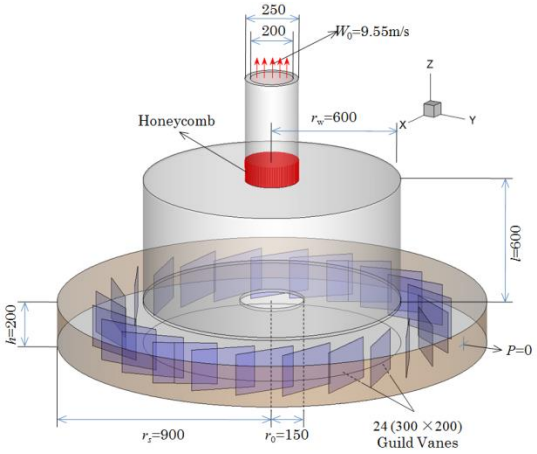

Fig. 1 The geometry of the model

When the centroid of the wall-adjacent cells falls within the logarithmic region of the boundary layer, the law-of-the-wall is employed as follows

$$\frac{\tilde{u}}{u_\tau} = \frac{1}{k}\ln E\left(\frac{\rho u_\tau y}{\mu}\right) \tag{6}$$

where $\tilde{u}$ is the filtered velocity tangential to wall, y is the distance between the center of the cell and the wall, u_τ is the friction velocity, and the constant E is 9.793.

2.2 Configurations of the numerical tornado simulator

In this study, a Ward-type simulator is chosen and the configurations of the model are shown in Fig. 1. The angular momentum of the flow entering into the convergence region is obtained by 24 guild vanes mounted on the ground at radius of 750 mm. The height of the guide vanes is 200 mm and the width is 300 mm. The angle of the guild vanes, θ, is 60°. The height of the inlet layer, h, and the radii of the updraft hole, r_0, are 200 mm and 150 mm respectively. The total outflow rate $Q = \pi r_t^2 W_0$ is held as a constant 0.3 m^3/s, where r_t is the radius of the exhaust outlet and W_0 is the velocity, 9.55 m/s, at the outlet. The dominant parameter determining the structure of a tornado-like vortex is identified as the *swirl ratio* and expressed as $S = \tan\theta/2a$, where a denotes the internal aspect ratio and equals to h/r_0. The local swirl ratio, S_c, defined by Lewellen *et al*. (2000), is calculated as 2.2. Another dimensionless parameter is the Reynolds number, $R_e = W_0 D/\upsilon$, where D is the diameter of the updraft hole. The maximum mean tangential velocity, V_c, in the cyclostrophic balance region is 8.33 m/s, and the radius, r_c, where the maximum mean tangential velocity occurs, is 32.6 mm.

2.3 Numerical scheme

Finite volume method is used for the present simulations. The second order central difference scheme is used for the convective and viscosity term, and the second order implicit scheme for the unsteady term. SIMPLE (semi-implicit pressure linked equations) algorithm is employed for solving the discretized equations (Ferziger and Peric 2002).

Table 1 Parameters used in this study

Angle of the guild vanes: θ	60^o	Reynolds number: $R_e = 2r_0W_0/\upsilon$	1.63×10^5
Height of the inlet layer: h	200 mm	Non-dimensional time step : $\Delta t W_0/2r_0$	0.032
Radius of the updraft hole: r_0	150 mm	Mesh size in the radial direction	2.0～26.0 mm
Radius of the exhaust outlet: r_t	100 mm	Mesh size in the vertical direction	1.0～5.0 mm
Velocity at the outlet: W_0	9.55 m/s	Mesh number	610497
Total outflow rate: $Q = \pi r_t^2 W_0$	0.3 m^3/s	Maximum mean tangential velocity: V_c	8.33 m/s
Internal aspect ratio: $a = h/r_0$	1.33	Radius of the core: r_c	32.6 mm
Swirl ratio: $S = \tan\theta/2a$	0.65		

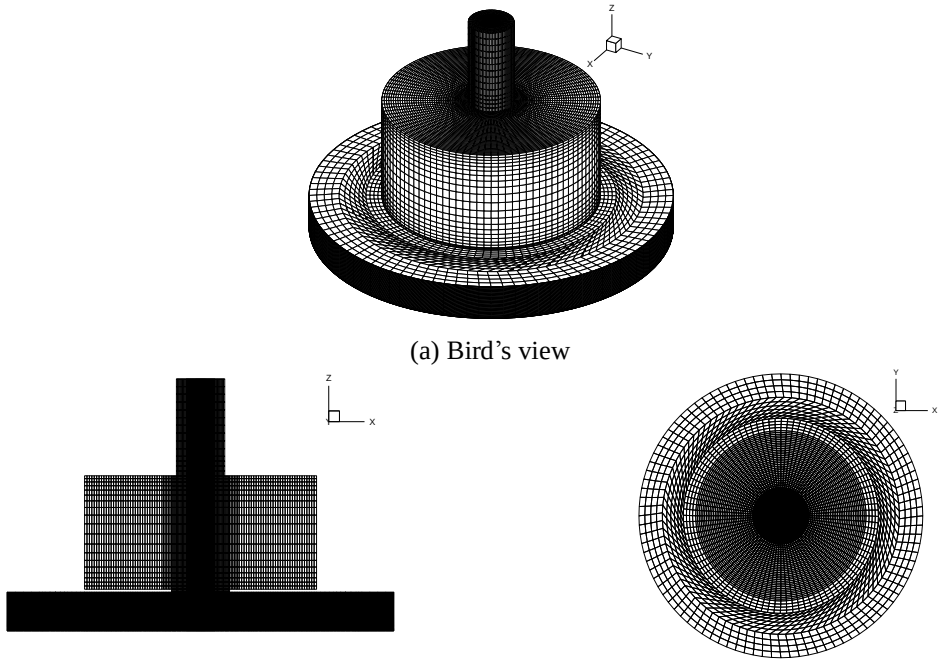

(a) Bird's view

(b) Side view

(c) Top view

Fig. 2 Mesh of the numerical model

At the inlet of the convergence region the pressure is set as zero. Uniform velocity boundary condition representative of the exhausting fan is specified at the outlet surface, where the radial, tangential and vertical velocities are 0, 0 and 9.55 m/s respectively. Non-slip boundary condition is applied at the bottom and the wall of the simulator. In most of the region, the wall-adjacent cells are in the laminar sublayer. The maximum of *y+* is 26 in the core region of the vortex. There are 7 grid points below the peak of mean radial velocity and 25 grid points below the peak of mean tangential velocity to make sure the boundary layer could develop properly.

A non-dimensional time step of 0.032 is adopted, calculated as $\Delta t W_0 / D$, where Δt is the time step. The numerical solution was carried out to 30s and the first 10s data were removed to eliminate the transit result. The data from 10s to 30s were applied to obtain the statistical information of the flow fields in the tornado-like vortex. The relative errors decrease with increasing in calculating time. For 20s, the relative error of the maximum mean tangential velocity in the cyclostrophic balance region becomes less than 1%.

Considering the axisymmetry of tornado-like vortex, a novel axisymmetric topology method is adopted, as shown in Fig. 2. With an intent to investigate the turbulent features in the vicinity of the center and the region near the ground, a fine mesh is considered in the domain of the convergence region, where 68 nodes in the radial direction and 25 nodes in the vertical direction are used, and the minimum size of the mesh are about 2 mm in the radial direction and 1mm in the vertical direction. The spacing ratios in the two directions are less than 1.2 in order to avoid a sudden change of the grid size. The total mesh number is about 6×10^5. Table 1 summarizes the parameters used in this study.

3. Turbulent characteristics

The turbulent characteristics of the tornado-like vortex with touching-down are summarized in this section. First, the profiles of the mean and the fluctuating velocities and pressure, as well as the turbulent kinetic energy (TKE) and the Reynolds shear stress uw are discussed. The calculation of the statistical values at each position is performed by averaging the values at the same radius and height over twelve azimuthal angles. Then, the force balances in radial and vertical direction are evaluated.

3.1 Turbulent flow fields

Fig. 3 shows the comparison of the flow fields in the laboratory tests by Matsui and Tamura (2009) and that in the numerical tornado simulator. Small particles are injected from the bottom in the numerical model with the objective of simulating the smoke used in the experiments. The flow fields are very turbulent and the core radii are almost same with each other.

The averaged flow fields on the horizontal cross-section of $z = 0.2r_c$ and vertical cross-section of $y = 0r_c$ are shown in Figs. 4(a) and 4(b) respectively. The axisymmetric flow pattern can be observed clearly in the horizontal cross-section with the center of the flow fields coinciding with that of the simulator. In the outside region, the significant radial component in addition to the tangential component indicates the feature of spiral motion which can be found from the streamlines superimposed on Fig. 4(a). On the vertical cross-section, at the center the flow moves downward, and near the ground a radial jet penetrates to the axis then turns upward. The radial jet

and the downward jet break away at the stagnation point, $r = 0$ and $z = 0.3r_c$, and a circulation zone is generated at the interface between the near-surface conical vortex and the aloft cylindrical vortex.

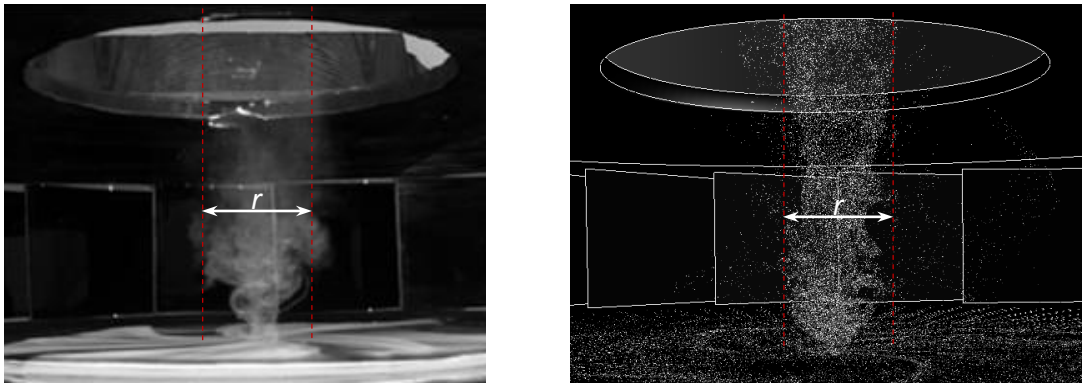

(a) Experiment (b) Simulation

Fig. 3 (a) Flow fields visualized by the smoke injected from bottom of the laboratory simulator and (b) flow fields visualized by small particles injected from the bottom of the numerical simulator

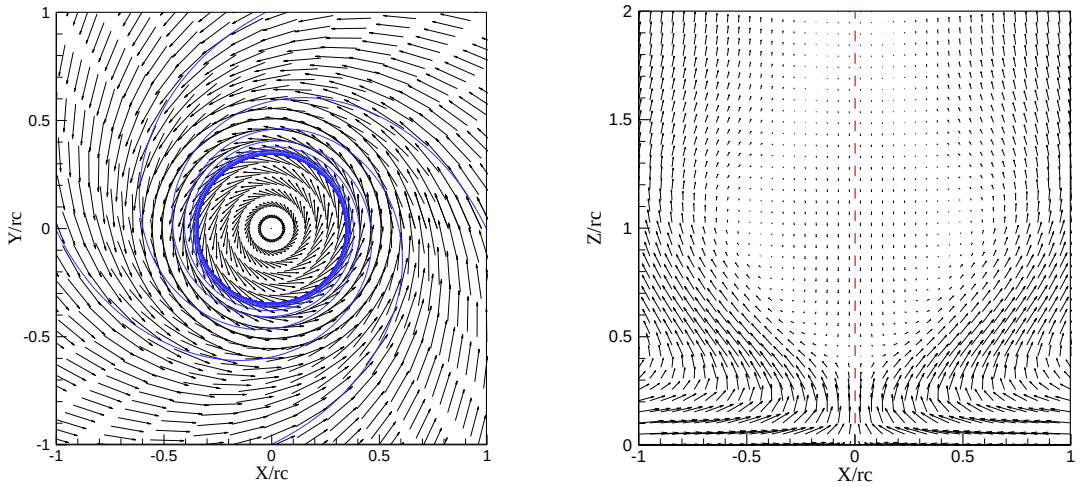

(a) $z = 0.2r_c$ (b) $y = 0r_c$

Fig. 4 Vectors of mean velocities on cross-sections of (a) $z = 0.2r_c$ and (b) $y = 0r_c$

The mean and fluctuating velocity profiles normalized by V_c at three elevations $z = 0.2r_c$, $z = 0.5r_c$ and $z = 2.0r_c$ are depicted in Fig. 5. Fig. 5(a) presents the mean radial velocity profiles. Major portion of the radial inflow is concentrated in a thin layer next to the ground which can be found in the profile at the elevation $z = 0.2r_c$. The concentration of the radial inflow will be explained by the force balance analysis in section 3.2. At the $r = 1r_c$, the maximum radial inward velocity reaches to about $0.7V_c$. The radial velocity decreases with the decreasing in radial distance and changes its sign near the center. At the height of $z = 0.5r_c$, the radial velocity shows positive sign in the core region, $r < 1r_c$, which can be explained like that the central downward flow meets upward flow and pushes the radial flow outward. Moving to high elevation, $z = 2.0r_c$, the flow reaches to the cyclostrophic balance, which means the centrifugal force due to the motion of the flow balances with the pressure gradient, and the direction of the motion of the flow should perpendicular to the direction of the pressure gradient, therefore the flow can only moves tangentially or vertically. This can be clearly found in the profile of the radial velocity at $z = 2.0r_c$ where the radial velocity is around 0. Fig. 5(b) shows the root mean square (r.m.s) of the fluctuating radial velocity, which increases with decrease in the radial distance at most elevations and shows peak in the center. It is noteworthy that, at $z = 0.5r_c$, u is almost a constant in the core region, which can be attributed to the mixing of the flow. At the center the r.m.s radial velocity shows large value while the mean radial velocity is zero. This will be explained in the following discussion about the dynamics of the tornado.

Normalized tangential velocities in respect to non-dimensional radial location are presented in Fig. 5(c). It is obvious that overall the maximum tangential velocity happens at $r = 1r_c$, except the locations close to the ground, where the tangential velocity increases to about 1.4 V_c at $r = 0.5r_c$. This increase in the tangential velocity is important for wind resistant design, since most of the engineering structures exist in the surface layer. Comparing the profiles of tangential velocity at high elevations, a shape similarity is revealed. The tangential velocity is initially zero at the center then increases to the maximum, for further increasing in radial distance it decreases. The profile of tangential velocity at $z = 1.67r_c$ is also plotted with the consideration of comparing the results by Matsui and Tamura (2009) and it shows good agreement with the experiment. The profiles of the r.m.s tangential velocity, v, is illustrated in Fig.5(d). Similar with the radial fluctuations, at most elevations the v shows the largest value at the center, while, at $z = 0.5r_c$, v is almost a constant along the radius from $r = 0$ to $r = 0.4r_c$. Same with the radial component, the generation of turbulence for the tangential components is completely different from that of the general turbulence whose source is mainly the velocity gradients as the fully developed boundary layer winds.

Fig. 5(e) shows the mean vertical velocities as a function of radial distance. The maximum axial velocity, $0.6V_c$, occurs at the center with a height of $0.2r_c$. This large axial velocity is attributed to the radial jet changing its direction to upward here. In the upper region, $z \geq 0.5r_c$, the vertical velocity first increases then decreases with decreasing in radial distance and the downward vertical velocity is observed at the center of the vortex. The normalized vertical velocities from the laboratory by Mitsuta and Monji (1984) are also plotted and the predicted velocities show satisfactory agreement with the measured ones at $z = 1.3r_c$. The profiles of w, resembles those of

the radial and tangential stresses in spite of the relatively smaller values, as shown in Fig. 5(f). Near the ground, $z = 0.2r_c$, w increases as decrease in the radial distance. The highest value of the r.m.s vertical velocity, $0.5V_c$, occurs at the center and another relatively large r.m.s vertical velocity occurs at $z = 0.5r_c$, $r = 0.4r_c$, where the strong mixing effects can be observed.

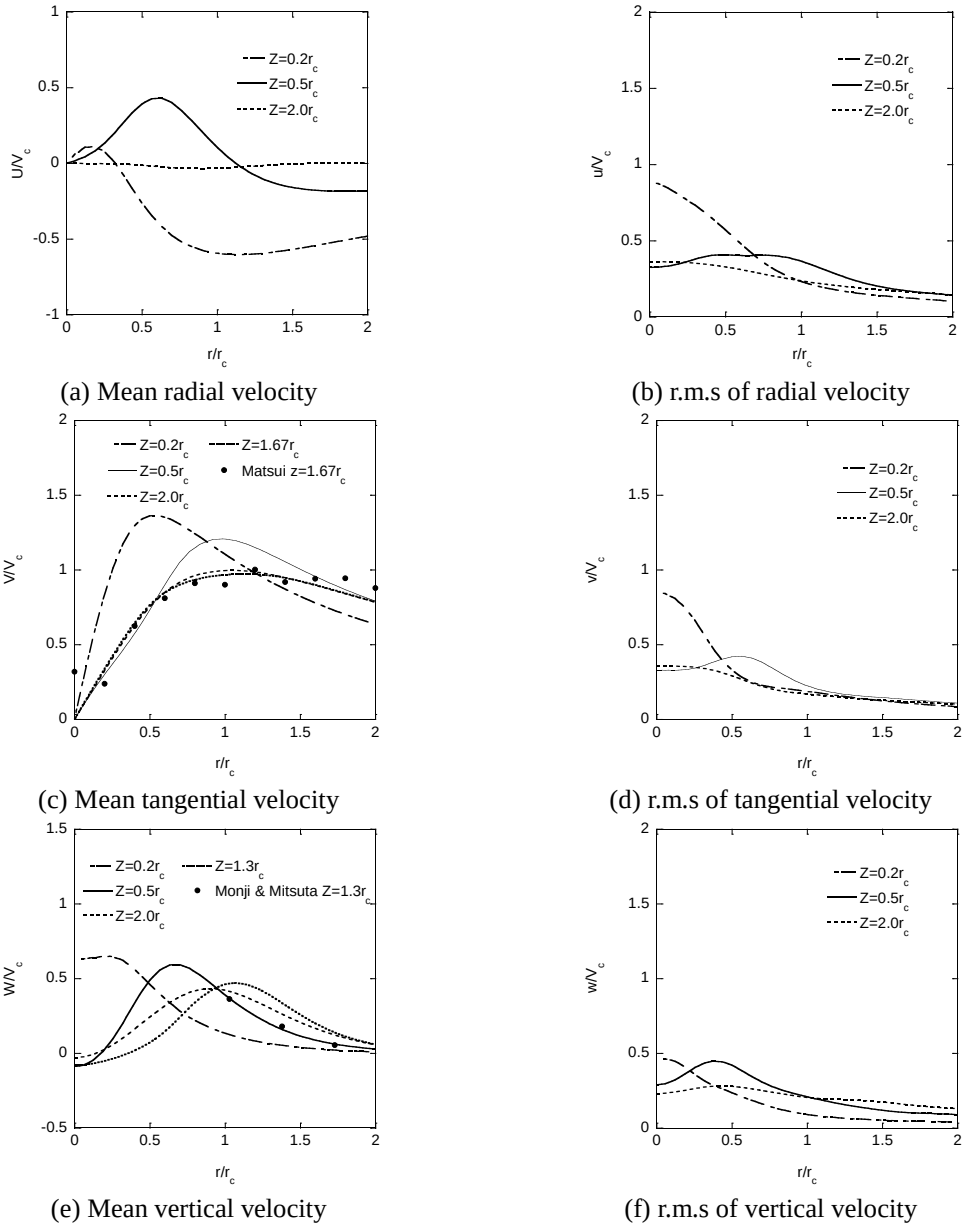

(a) Mean radial velocity (b) r.m.s of radial velocity

(c) Mean tangential velocity (d) r.m.s of tangential velocity

(e) Mean vertical velocity (f) r.m.s of vertical velocity

Fig. 5 Normalized mean velocity and r.m.s of the fluctuating velocities at three vertical positions. (a) mean radial velocity, (b) r.m.s of radial velocity, (c) mean tangential velocity, (d) r.m.s of tangential velocity, (e) mean vertical velocity, and (f) r.m.s of vertical velocity

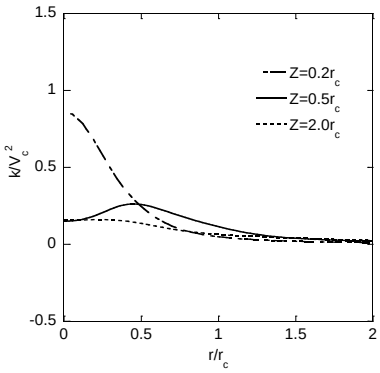

(a) Turbulent kinetic energy k

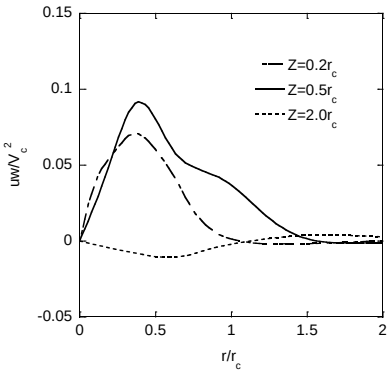

(b) Reynolds stress uw

Fig. 6 Horizontal distribution of (a) turbulent kinetic energy k and (b) Reynolds stress uw

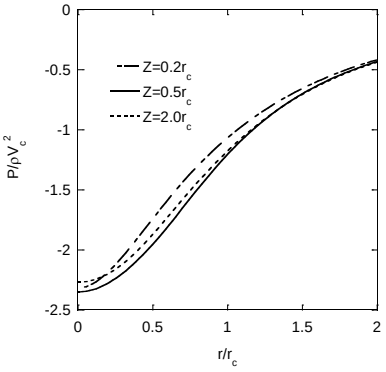

(a) Mean pressure

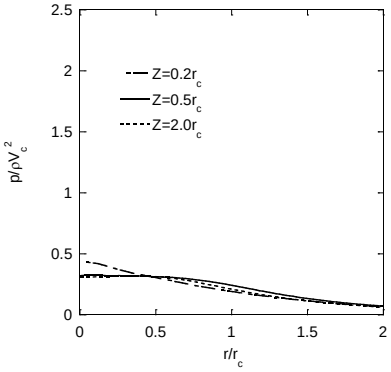

(b) r.m.s of the pressure fluctuation

Fig. 7 Horizontal distribution of (a) mean pressure and (b) r.m.s of the pressure fluctuation

The horizontal distributions of the normalized turbulent kinetic energy, k , are shown in Fig. 6(a). The maximum turbulent kinetic energy is about 0.8 occurring at the axis with a height of 0.2 r_c , and the generation of the turbulent kinetic energy comes mainly from the radial and tangential fluctuating velocities. The zero values for the mean radial and tangential velocities along the central line lead to the conclusion the turbulence in the center plays the dominant role for the damages associated to the tornado events.

Another important variable used to analyze turbulence is the Reynolds shear stress, thus the profiles of the normalized Reynolds shear stress, uw are also presented in Fig. 6(b). Compared with the normal stresses, the shear stress is less than the normal stresses with one order of magnitude. In addition, at the central line the shear stress is zero, while the normal stresses show maximum values.

Fig. 7(a) illustrates the variations of the normalized mean pressure. Different with the velocity components, the profiles of the pressure show almost same shapes at various elevations. As closing

to the central axis, significant pressure drop is observed. The horizontal distributions of the r.m.s for the pressure fluctuation, p_{rms}, are illustrated in Fig. 7(b), which shows the maximum value of 0.45 at the height of 0.2 r_c, and the magnitude is much smaller than that of the mean pressure at all locations.

3.2 Force balances in radial and vertical direction

The radial and vertical force balances in tornado-like vortex are investigated by using the time-averaged axisymmetric Navier-Stokes equations as shown by Ishihara *et al*. (2011). The sub-terms of the turbulent are also analyzed in detail to examine how the turbulence influences the mean flow fields.

The time-averaged Navier-Stokes equation in radial direction can be expressed as

$$U\frac{\partial U}{\partial r}+W\frac{\partial U}{\partial z}-\frac{V^2}{r}=-\frac{1}{\rho}\frac{\partial P}{\partial r}-\left(\frac{\partial u^2}{\partial r}+\frac{\partial uw}{\partial z}-\frac{v^2}{r}+\frac{u^2}{r}\right)+D_u \tag{7}$$

The left hand side consists of the radial advection term, A_{ru}, the vertical advection term, A_{zu}, as well as the centrifugal force term, C_{r}. The right hand side of the equation is the radial pressure gradient term, P_{r}, turbulent force term, T_{u}, and the diffusion term, D_{u}. The sub-terms in the turbulent force are T_{ru2}, T_{zuw}, T_{v2} and T_{u2}. The diffusion term in the equation is small enough and can be ignored comparing with the other terms. The terms of $-V^2/r$, $-v^2/r$ and u^2/r at the central line are calculated by the method as described in Appendix.

Force balance in the radial time-averaged Navier-Stokes equation at $z=0.2r_c$ is shown in Fig. 8(a), which reveals that the centrifugal force, pressure gradient and the vertical advection terms are the significant portion of the total balance and the turbulent force plays little role. Centrifugal force is the largest term in the corner region, which increases with decreasing in radius until reaching to the maximum at around $r=0.4r_c$ and then eventually reaches to 0 at the center of vortex. The magnitudes of vertical advection term and the pressure gradient term have a similar tendency with the centrifugal force, and the magnitude of the vertical advection term is larger than that of the pressure gradient term for $r>0.7r_c$.

With an attempt to investigate the turbulent force in detail, the variations of the sub-terms in the turbulent force versus radius are illustrated in Fig. 8(b). Two sub-terms, T_{v2} and T_{u2}, are extremely large in comparison with the other terms and an acute increase of the magnitudes of T_{v2} and T_{u2} in the corner region is observed. The non-zero r.m.s of the fluctuating velocities provides that T_{v2} and T_{u2} reach to infinite at the center, but they almost cancel out with each other. The reason will be explained in the section 4.1.

The tangential velocity can be estimated from the balance between the centrifugal force, pressure gradient and the vertical advection terms as follows

$$V_{P+A}=\sqrt{V_P^2+V_A^2}=\sqrt{\frac{1}{\rho}\frac{\partial P}{\partial r}r+W\frac{\partial U}{\partial z}r} \tag{8}$$

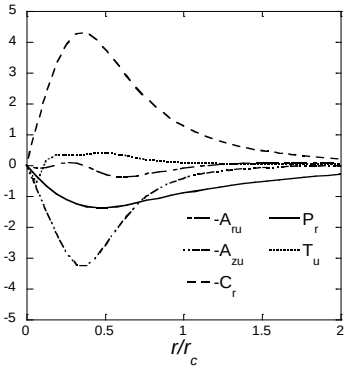

(a) Advection, pressure gradient, centrifugal force and turbulence terms

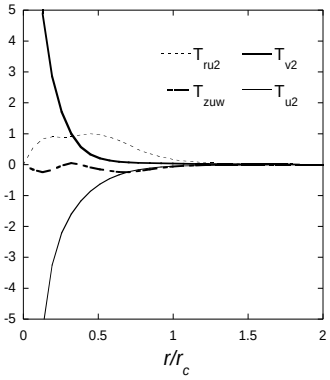

(b) Sub-terms of turbulent force

Fig. 8 Radial distribution of normalized radial force terms at $z = 0.2r_c$, with (a) representing advection, pressure gradient, centrifugal force and turbulence terms, and (b), the sub-terms of turbulent force

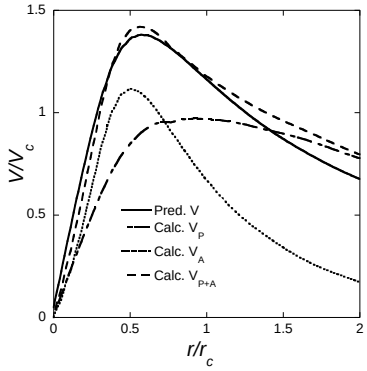

Fig. 9 Comparison of simulated and calculated tangential velocities at $z = 0.2r_c$

where, V_P and V_A are calculated as $\sqrt{1/\rho \cdot \partial P/\partial r \cdot r}$ and $\sqrt{W \cdot \partial U/\partial z \cdot r}$. The calculated tangential velocity based on the model shows good agreement with the simulated one as shown in Fig. 9. This indicates that the increase of tangential velocity near the surface comes from not only the pressure gradient term, P_r, but also the vertical advection term A_{zu}. The mechanism of the flow fields can be explained such that pressure gradient is independent of the height and the ground pressure gradient does not balance with the centrifugal force because of the friction. As a result, large radial inflow occurs near the ground and causes an increase in the tangential velocity there.

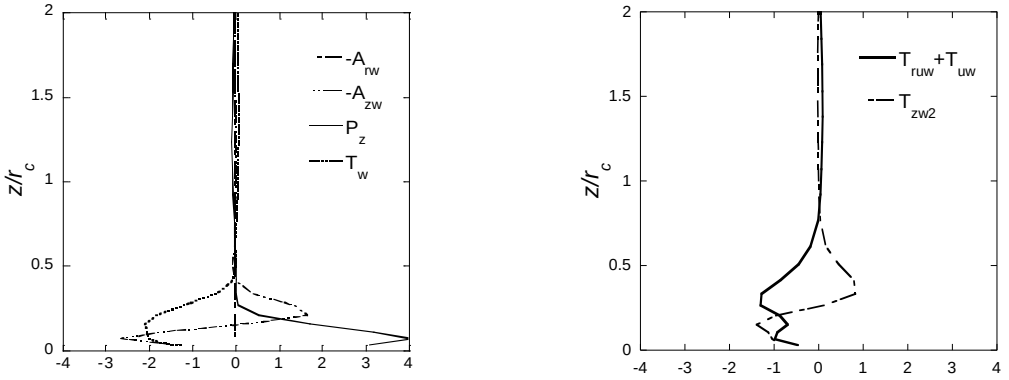

(a) Advection, pressure gradient and turbulence terms (b) Sub-terms of turbulent force

Fig. 10 Vertical distribution of normalized vertical force terms at $r = 0r_c$, with (a) representing advection, pressure gradient and turbulence terms, and (b), the sub-terms of turbulent force

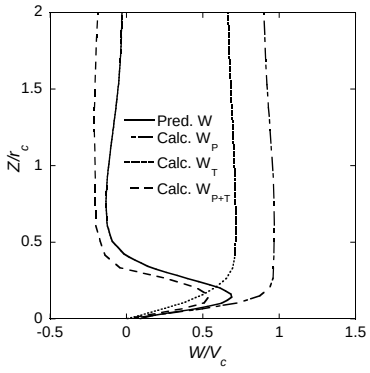

Fig. 11 Comparison of simulated and calculated vertical velocities at $r = 0r_c$

The time-averaged Navier-Stokes equation in the vertical direction can be expressed as

$$U\frac{\partial W}{\partial r}+W\frac{\partial W}{\partial z}=-\frac{1}{\rho}\frac{\partial P}{\partial z}-\left(\frac{\partial uw}{\partial r}+\frac{\partial w^2}{\partial z}+\frac{uw}{r}\right)+D_w \tag{9}$$

The left hand side consists of the radial advection term, A_{rw}, and the vertical advection term, A_{zw}. The right hand side is the radial pressure gradient term, P_{z}, turbulent force term, T_{w}, and the diffusion term, D_{w}. The sub-terms in the turbulent force are T_{ruw}, T_{zw2} and T_{uw}. The diffusion term in the equation is small enough and can be ignored compared with the other terms. $\partial uw/\partial r$ and uw/r at the central line are calculated as shown in Appendix.

Fig. 10 (a) shows the balance of the vertical force in the vertical time-averaged Navier-Stokes equation at the center of vortex. It is observed that the vertical advection term balances mainly

with the pressure gradient term and the turbulent force term. The radial advection term is zero at all heights in respect of the symmetry of the mean vertical velocity. The vertical advection term becomes alternately positive and negative with height, and the height of the inversion point in the profile is $0.15\,r_c$. The magnitudes of the pressure gradient and the turbulent force exhibit a similar tendency, first increase then decrease with decreasing in height and the maximum values occur in the region below the height of $0.2\,r_c$. Above the height of $0.4\,r_c$, all the terms are almost zero on account of the relatively stable flow fields in the upper part of the vortex.

The sub-terms of turbulent force at $r = 0r_c$ are illustrated in Fig. 10(b). Above the height of $0.7\,r_c$, the sub-terms are about zero. Within the height between $0.7\,r_c$ and $0.4\,r_c$ the non-zero sub-terms almost cancel out with each other. Near the ground, the sum of $\partial uw/\partial r$ and uw/r shows negative value, while the sub-term $\partial w^2/\partial z$ changes from negative to positive with height.

The vertical velocity can be estimated from the balance between vertical advection term, the pressure gradient term and the turbulent force term as follow

$$W = \begin{cases} \sqrt{W_P^2 + W_T^2} = \sqrt{2\dfrac{P_S - P}{\rho} - 2\int_0^z T_w dz} & for \quad W \geq 0 \\ -\sqrt{W_P^2 + W_T^2} = -\sqrt{2\dfrac{P_S - P}{\rho} - 2\int_0^z T_w dz} & for \quad W < 0 \end{cases} \tag{10}$$

where, the W_P and W_T are calculated as $\sqrt{2(P_S - P)/\rho}$ and $\sqrt{2\int_0^z T_w dz}$, P_S is the pressure at surface and P is the pressure at the height of z. The sign of W can be decided as follows: W has to be positive at the level very close to the bottom, since it is impossible for the particles to move downward here. With increasing in elevation, W will be 0 at some height and should be negative further increase in elevation. The estimated tangential velocity W based on the model shows favorably agreement with the simulated one as shown in Fig. 11. The vertical velocity, W_P, is larger than the simulated result, if the turbulent contribution is not taken into consideration. This indicates that the pressure gradient accelerates the vertical velocity while the turbulent force decelerates that.

4. Dynamics of the tornado-like vortex

The Dynamics of tornado-like vortex with touching down are revealed in this section. Firstly, the flow pattern of the instantaneous flow fields is examined by the pressure iso-surface, the vectors as well as the time series of velocities. Then the power spectrums for the fluctuating velocities are studied to quantify the organized swirl motion of the tornado-like vortex. Finally, the gust speed of tornado-like vortex with touching down is calculated to provide valuable information from an engineering point of view. In the following discussions the time is normalized by $2\pi r_c/V_c$, which is the period of the vortex based on the assumption of the solid rotation in the core where the mean tangential velocity is proportional to the radial distance.

4.1 Instantaneous flow fields

The three-dimensional pressure iso-surfaces of $0.7\,P_{\min}$ are illustrated in Fig. 12, where $P_{\min}$ is the minimum pressure of the flow fields. The pressure iso-surfaces yield the familiar and clear shape of the tornado. It is apparent that the center of the vortex is not stationary but associated with a swirl motion around the center of the simulator as shown by the points in Fig. 12. The vortex reaches to the southern, eastern, northern and western sides at t =1033.2, 1036.6, 1039.5 and 1042.1 respectively, implying that the angular speed of the swirl motion is much lower than that of the solid rotation. The swirl motion is found to be organized rather than random or chaotic, which will be clarified in the spectrum analysis. At the corner of the vortex, some small eddies appear with fairly rapid evolution and they locate primarily inside the core of the vortex.

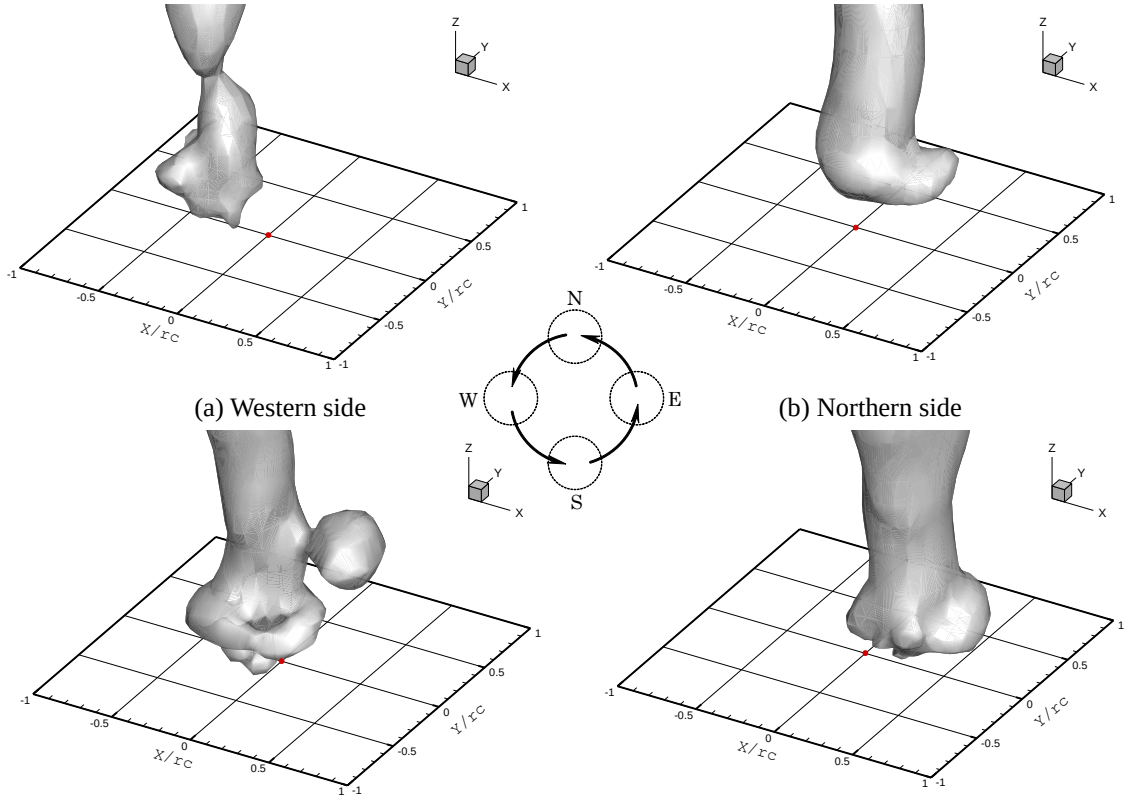

(a) Western side (b) Northern side

(c) Southern side (d) Eastern side

Fig. 12 Evolution of three-dimensional pressure contour with pressure level of $0.7\,P_{\min}$ for one period. Vortex center moves from (c) southern side at t =1033 to (d) eastern side at t =1036.6, (b) northern side at t =1039.5 and (a) the western side at t =1042

Fig. 13 shows the instantaneous velocity vectors at the horizontal cross-section of $z = 0.2r_c$. The velocity vectors are not as symmetry as that in Fig. 4(a), and the swirl motion can be clearly observed, where the direction of the wind velocity at the center changes periodically due to this swirl motion. When the tornado-like vortex moves to the southern and the northern sides, the velocity vectors are almost parallel to the *x* axis at the center, indicating the occurrence of the large radial speed and the small tangential speed, as shown in Figs. 13(c) and 13(b). On the other hand, when the vortex moves to the eastern and western sides, the velocity vectors are almost perpendicular to the *x* axis at the center, which means a small radial speed and a large tangential speed occur, as shown in Figs. 13(d) and 13(a). Hence, the time histories of the radial and the tangential velocities should be periodic. As a result, it can be concluded that the turbulence in the tornado-like vrotex is different from the turbulence in the full developed shear layer and the main source of the fluctuationg horizontal velocities in the tornado-like vortex is the organized swirl motion.

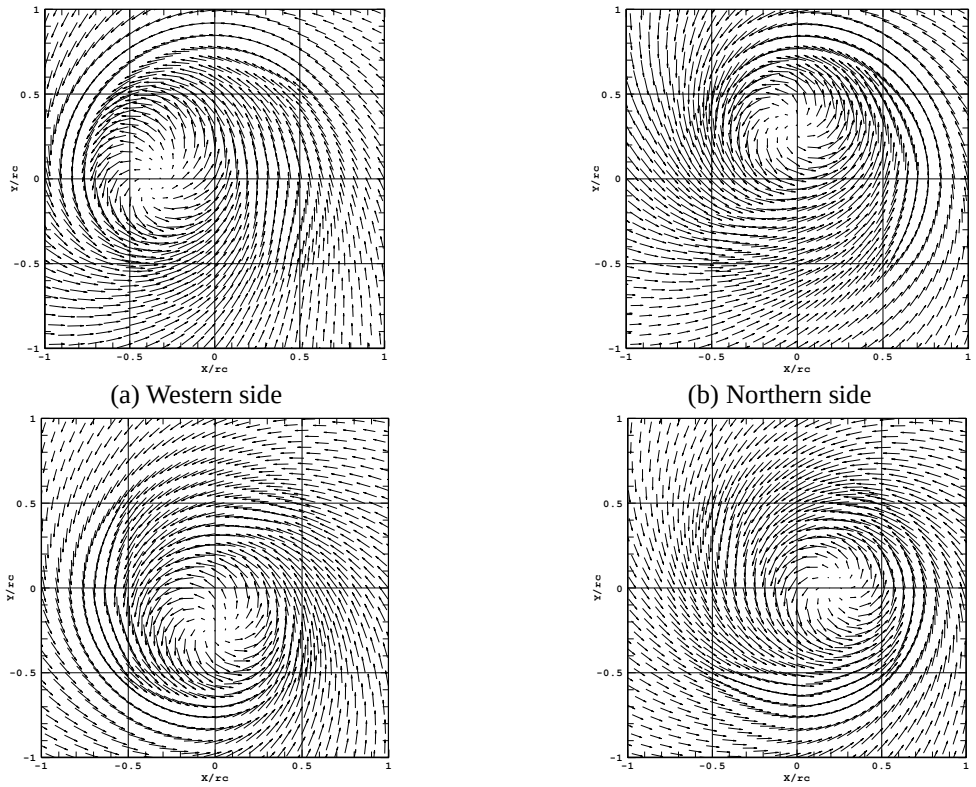

(a) Western side (b) Northern side

(c) Southern side (d) Eastern side

Fig. 13 Vector fields at the cross section of $z = 0.2r_c$ for one period. Vortex center moves from (c) southern side at t =1033 to (d) eastern side at t =1036.6, (b) northern side at t =1039.5 and (a) the western side at t =1042

Sample traces of radial and tangential velocity fluctuations from non-dimensional time 1032 to 1044 at the location of $r = 0r_c$ and $z = 0.2r_c$ are shown in Fig. 14. The vertical dashed lines show the time as the tornado-like vortex moves to the southern, eastern, northern and western sides. It is observed that the tangential and radial velocities display significant fluctuations due to the organized swirl motion. The shapes of the time histories for radial and tangential velocities are similar and periodic. Moreover, the large values of the radial and tangential velocities do not happen simultaneously. When the tornado-like vortex moves to the eastern and western sides, the tangential wind speed is larger than the radial wind speed, on the other hand when the vortex moves to the southern and northern sides, the tangential wind speed is smaller than the radial wind speed, as shown by the points in Fig. 14 indicating a 90^o phase difference between the time histories of the radial and tangential velocities. The sinuous shape for the radial and tangential velocities yields zero time-averaged values and almost the same standard deviations. This is the reason why the sub-terms v^2/r and u^2/r cancel out with each other in the radial force balance at the center.

Fig. 15 shows the time series of the vector distributions at the cross-section of *y*=0. The dashed line shows the axis of the simulator. The vertical velocity at the central line does not change dramatically at each elevation, which can be explained as such that, even though the organized swirl motion exists, the distance between the center of the simulator and the center of the instanteneous vortex does not vary a lot, maintaining $0.25\,r_c$ approximately as shown in Fig. 13.

The comparison between the time variations of the instantaneous radial and vertical velocity fluctuations from non-dimensional time 1032 to 1044 at the location of $r = 0r_c$ and $z = 0.2r_c$ is shown in Fig. 16. The pretty small and random fluctuation of the vertical component is the indicative and the correlation between the organized swirl motion and the vertical velocity fluctuation is not obvious. It can be concluded that the organized swirl motion is not the main source of the turbulence for the vertical velocity. As for the effectiveness of turbulent mixing, the vertical velocity is smaller than that caused by the laminar vortex. This is the reason why the turbulent force decreases the vertical velocity.

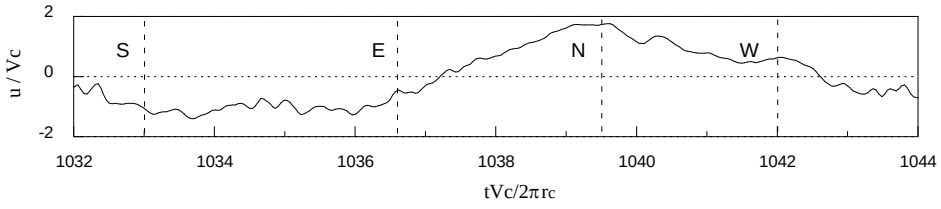

(a) Radial velocity

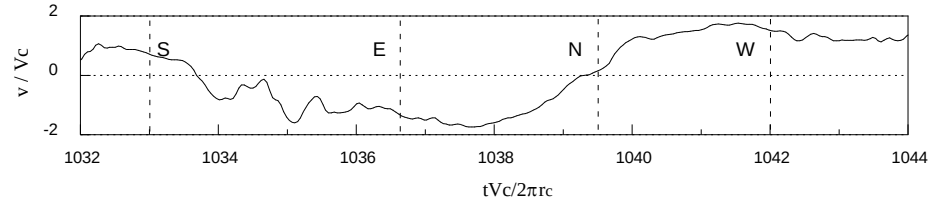

(b) Tangential velocity

Fig. 14 Simultaneous traces of instantaneous (a) radial velocity and (b) tangential velocity

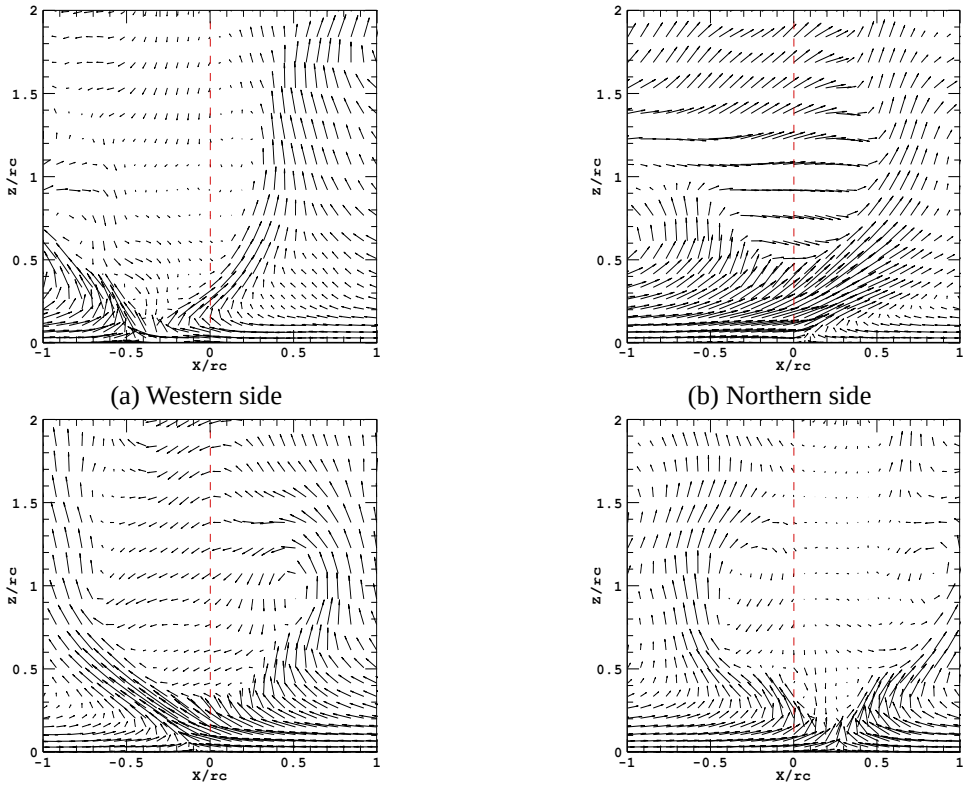

(a) Western side (b) Northern side

(c) Southern side (d) Eastern side

Fig. 15 Vector fields at the cross section of y=0 for one period. Vortex center moves from (c) southern side at t=1033 to (d) eastern side at t=1036.6, (b) northern side at t=1039.5 and (a) the western side at t=1042

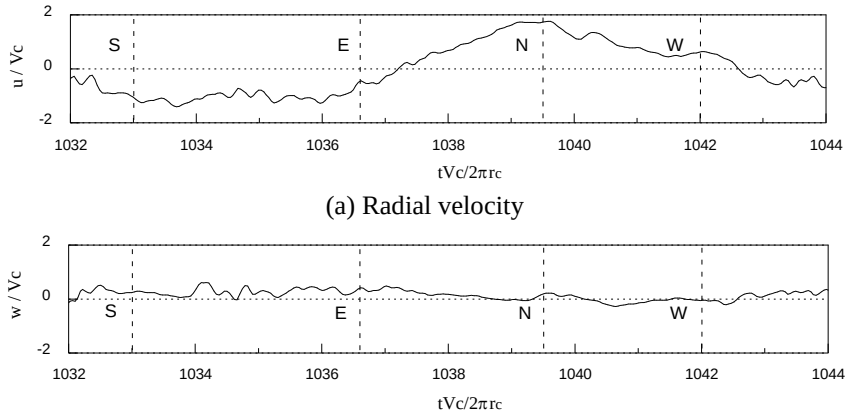

(a) Radial velocity

(b) Vertical velocity

Fig. 16 Simultaneous traces of instantaneous (a) radial velocity and (b) vertical velocity

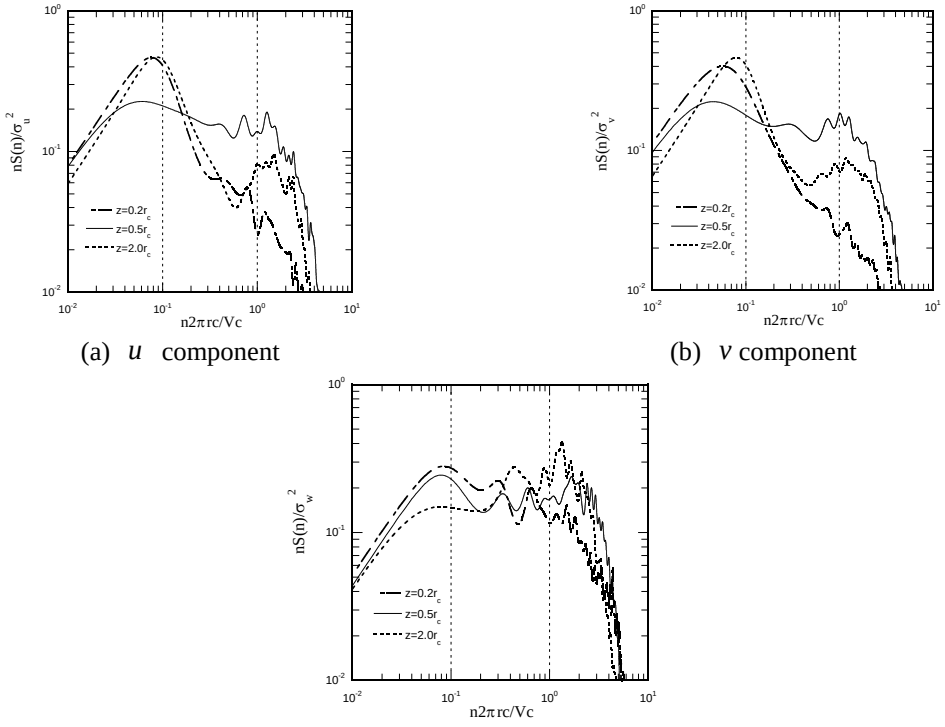

(a) u component (b) v component

(c) w component

Fig. 17 Normalized spectral densities of velocity fluctuations at $r = 0rc$, (a) u component and (b) v component, (c) w component

4.2 Spectrum analysis

In order to quantify the organized swirl motion of the tornado-like vortex, the power spectra of the velocity fluctuations, u, v, w, is calculated by the Maximum Entropy Method (MEM). The normalized spectra of radial, tangential and vertical components against a non-dimensional frequency $f = n2\pi r_c / V_c$, where n is the natural frequency in Hz, at r =0 and $r = 1r_c$ are illustrated respectively in Fig. 17.

The u spectra at radius of r =0 is shown in Fig. 17(a). At the height of $0.2\,r_c$ the only one peak at about f =0.08 is observed which corresponds to the organized swirl motion and the primary energy of the fluctuating radial velocity comes mainly from the swirl motion. At the height of $0.5\,r_c$, there is no apparent peak for the radial component, due to the strong mixing of the fluids. Compared with the data at $z = 0.2r_c$, the primary frequency at $z = 2r_c$ shifted slightly toward the high frequency range and there is another peak at about f =1, coresponding to the rotation of the core of the tornado. The v spectra at radius of r =0 shown in Fig. 17(b) are similar with those of u component and the fluctuating energy is concentrated in the low frequency range. This fact implies that the fluctuating tangential and radial velocities come mainly from the swirl motion. In comparison with the radial and tangential components, the spectra of the

vertical velocity as shown in Fig. 17(c) are broad, indicating that the fluctuating vertical velocity is not organized as the horizontal velocity components. Moreover, at high elevation, $z = 2r_c$, the fluctuating energy is concentrated in the high frequency range and has a peak at about f =1, indicating that the fluctuating vertical velocity is mainly attributed to the rotation of the core of the tornado at high elevations.

4.3 Gust speeds

The gust speed is the governing factor in the structure design, which is often referred to as a "3-second gust". In this study, the time used to calculate the gust speed is based on the time scale, as shown in Table 2, where λ_l , λ_v and λ_t denote the length scale, velocity scale and time scale respectively. The information of the tornado in nature is provided by the DOW radar dataset (Dowell *et al*. 2005).

Fig. 18 shows the normalized mean speeds, the speed standard deviations and the gust speeds at $r = 0r_c$ and $r = 0.5r_c$ with a height of $0.2\,r_c$. It is noteworthy to mention that the gust speed is 1.7 times the maximum mean tangential velocity, V_c, at the center, even though the mean speed is zero, indicating that the velocity fluctuation by the swirl motion can cause a large gust speed. The mean speed and the gust speed increase to 1.4 V_c and $1.9V_c$ at $r = 0.5r_c$, whereas the standard deviation decreases to $0.3V_c$, hence the gust speed comes mainly from the mean speed. The high gust speed is the explanation why tornados cause tremendous destructions near the central region.

Table 2 Scale ratio of tornado in nature to simulated tornado

	Real tornado	Numerical tornado	Scale ratio
r_c (m)	200	0.0326	λ_l = 6134
V_c (m/s)	65	8.33	λ_v = 7.8
Averaging Time (s)	3	0.0038	λ_t = 786

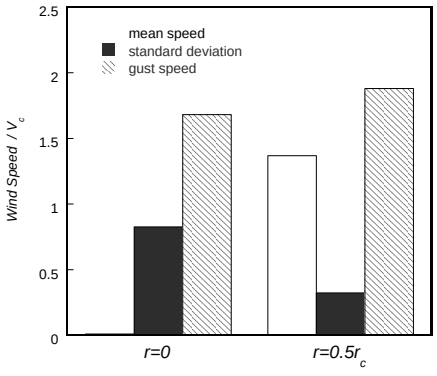

Fig.18 Mean speed, standard deviation and gust speed at two representative locations

5. Conclusions

The three-dimensional turbulent flow field and dynamics of a tornado-like vortex with touching down are investigated by using LES turbulence model. The conclusions of this study are summarized as follows:

- A numerical tornado simulator developed in this study successfully generates tornado vortex with touching down and shows a good agreement with those from the laboratory simulator. The tangential velocity reaches to 1.4 V_c at $r = 0.5r_c$ near the ground and the radial inflow is concentrated in a thin layer near the ground, showing the peak radial inward velocity of about 1 V_c at $r = 1r_c$. The turbulent kinetic energy gives a maximum value at the center of vortex, while the shear stress at the central line is zero.
- The increase of tangential velocity near the ground and the upward-downward vertical velocity at the center of vortex can be well explained by axisymmetric time-averaged N-S equation. The turbulent force plays little role in the radial balance, but that could not be neglected in the vertical balance.
- The vortex with touching down is associated with a swirl motion, which is organized instead of random and it is the main source of the turbulence of the radial and tangential components, also the explanation why the turbulent contribution is negligible in the radial balance.
- Two typical peaks are observed from the power spectra of the velocity fluctuations associated with organized swirl motion of the tornado-like vortex. One appeared at about f = 0.08 at the level close to the ground corresponds to the organized swirl motion and another peak at about f = 1 corresponds to the rotation of the core of the tornado.
- The gust speed at the center of the vortex is 1.7 V_c even though the mean speed is zero, while the gust speed at $r = 0.5r_c$ comes mainly from the mean speed. The high gust speed is the explanation why tornados cause tremendous destructions in the central region.

References

Baker, G.L. (1981), *Boundary layer in a laminar vortex flows*, PhD Thesis, Purdue University, West Lafayette, IN USA.

Dowell, D.C., Alexander, C.R., Wurman, J.M. and Wicker, J.L. (2005), "Centrifuging of hydrometeor and debris in tornadoes: radar-reflectivity patterns and wind-measurement erros", *Mon. Weather Rev.*, **133**, 1501-1524.

Ferziger, J. and Peric, M. (2002), *Computational method for fluid dynamics*, 3rd Ed., Springer.

Haan, F.L., Sarkar, P.P. and Gallus, W.A. (2008), "Design, construction and performance of a large tornado simulator for wind engineering applications", *Eng. Struct.*, **30**(4), 1146-1159.

Howells, P.C., Rotunno, R. and Smith, R.R. (1988), "A comparative study of atmospheric and laboratory analogue numerical tornado-vortex models", *Q. J. Roy. Meteor. Soc.*, **114**(481) , 801-822.

Ishihara, T., Oh, S. and Tokuyama, Y. (2011), "Numerical study on flow fields of tornado-like vortices using the LES turbulent model", *J. Wind Eng. Ind. Aerod.*, **99**(4), 239-248.

Kuai, L., Haan, F.L., Gallus, W.A. and Sarkar, P.P. (2008), "CFD simulations of the flow field of a laboratory-simulated tornado for parameter sensitivity studies and comparison with field measurements", *Wind Struct.*, **11**(2), 75-96.

Lewellen, D.C., Lewellen, W.S. and Sykes, R.I. (1997), "Large-eddy simulation of a tornado's interaction with the surface", *J. Atmos. Sci*. **54**(5), 581-605.

Lewellen, D.C., Lewellen, W.S. and Xia. J. (2000), "The influence of a local swirl ratio on tornado intensification near the surface", *J. Atmos. Sci*, **57**(4), 527-544.

Lewellen, D.C. and Lewellen, W.S. (2007), "Near-surface intensification of tornado vortices", *J. Atmos. Sci*,, **64**(7), 2176-2194.

Liu, Z. and Ishihara, T. (2012), "Effects of the Swirl Ratio on the Turbulent FlowFields of Tornado-like Vortices by using LES Turbulent Model", *Proceedings of the 7th International Colloquium on Bluff Body Aerodynamics and Applications*, CD-ROM.

Matsui, M. and Tamura, Y. (2009), "Influence of swirl ratio and incident flow conditions on generation of tornado-like vortex", *Proceedings of the EACWE 5*, CD-ROM.

Mitsuta, Y. and Monji, N. (1984), "Development of a laboratory simulator for small scale atmospheric vortices", *Nat. Disaster Sci.*, **6**, 43-54.

Natarajan, D. and Hangan, H. (2012), "Large eddy simulation of translation and surface roughness effects on torando-like vortices", *J. Wind Eng. Ind. Aerod.*, **104-106**, 577-584.

Nolan, D.S. and Farrell, B.F. (1999), "The structure and dynamics of tornado-like vortices", *J. Atmos. Sci*., **56**(16), 2908-2936.

Oka, S. and Ishihara, T. (2009), "Numerical study of aerodynamic characteristics of a square prism in a uniform flow", *J. Wind Eng. Ind. Aerod*., **97**(11-12), 548-559.

Tari, P.H., Gurka, R. and Hangan, H. (2010), "Experimental investigation of tornado-like vortex dynamics with swirl ratio: The mean and turbulent flow fields", *J. Wind Eng. Ind. Aerod*., **98**(12), 936-944.

Wan, C.A. and Chang, C.C. (1972), "Measurement of the velocity field in a simulated tornado-like vortex using a three-dimentional velocity probe", *J. Atmos. Sci*., **29**(1), 116-127.

Ward, N.B. (1972), "The exploration of certain features of tornado dynamics using a laboratory model", *J. Atmos. Sci.*, **29**(6), 1194-1204.

Wilson, T. and Rotunno, R. (1986), "Numerical simulation of a laminar end-wall vortex and boundary layer", *Phys. Fluids*, **29**(12), 3993-4005.

CC

Appendix

The following introduces the method calculating $-V^2/r$, $-v^2/r$ and u^2/r in the radial axisymmetric Navier-Stokes equation and $\partial uw/\partial r$ and uw/r in vertical axisymmetric Navier-Stokes equation at the central line. The subscripts r, θ, x and y are adopted to distinguish the radial and tangential variables in cylindrical coordinate as well as the variables in *x* and *y* directions in Cartesian coordinate.

The mean tangential velocity is assumed to be nearly proportional to the radius near the center of the vortex (see Ishihara *et al*. (2011)) and can be expressed as

$$V = \alpha r \tag{A.1}$$

where α is a constant. The centrifuge force, V^2/r, equals to $\alpha^2 r$ near the center and approaches to 0 at the center of the vortex.

Table A1. Symmetries of variables in Cartesian coordinate

	u_x^2	v_y^2	w_z^2	$u_x v_y$	$u_x w_z$	$v_y w_z$
Cartesian coordinate	S	S	S	S	A	A

*S and A denote symmetry and asymmetry with respect to *x* and *y* axes, respectively

The turbulent force for the radial axisymmetric Navier-Stokes equation should equal to that for Cartesian Navier-Stokes equation in x direction at the center

$$\frac{\partial u^2}{\partial r} + \frac{\partial uw}{\partial z} - \frac{v^2}{r} + -\frac{u^2}{r} = \frac{\partial u_x^2}{\partial x} + \frac{\partial u_x v_y}{\partial y} + \frac{\partial u_x w_z}{\partial z} \tag{A.2}$$

According to the symmetry of the Reynolds stresses, as illustrated in Table A1, $\partial u_x^2/\partial x$ and $\partial u_x v_y/\partial y$ should equal to 0, and $\partial uw/\partial z$ should equal to $\partial u_x w_z/\partial z$, so the sum of turbulent terms, $\partial u^2/\partial r - v^2/r + u^2/r$, equals to 0.

The turbulent force for the vertical axisymmetric Navier-Stokes equation should equal to those for Cartesian Navier-Stokes equation in *z* direction at the center

$$\frac{\partial uw}{\partial r} + \frac{uw}{r} + \frac{\partial w^2}{\partial z} = \frac{\partial u_x w_z}{\partial x} + \frac{\partial v_y w_z}{\partial y} + \frac{\partial w_z^2}{\partial z} \tag{A.3}$$

$\partial w^2/\partial z$ should equal to $\partial w_z^2/\partial z$, $\partial uw/\partial r + uw/r$ can be calculated by $\partial u_x w_z/\partial x + \partial v_y w_z/\partial y$.